Longitudinal registration of human fetal brain MRI

Florian Scalvini[1], Anne Kerachni[1], François Rousseau[1], and Nicolas Passat[2]

[1] IMT Atlantique, LaTIM U1101 INSERM, Brest, France
firstname.lastname@imt-atlantique.fr
[2] Université de Reims Champagne-Ardenne, CRESTIC, Reims, France
nicolas.passat@univ-reims.fr

Abstract. Longitudinal Magnetic Resonance Imaging (MRI) coupled with image registration approaches is a well-established approach for estimating spatio-temporal brain development. We present a study of diffeomorphic registration paradigms abilities for modelling fetal brain deformations during cortical gyrification. We investigate how the use of longitudinal MRI sequences can improve the accuracy of deformation estimates. First, we introduce an approach that integrates multiple time points into a stationary velocity field (SVF)-based longitudinal registration framework, enabling to model continuous spatio-temporal deformations from the full MRI sequence. Second, we assess this approach alongside existing diffeomorphic registration methods on two fetal brain atlases, evaluating their ability to capture the dynamic processes of fetal cortical maturation. Our results show that even though all evaluated methods systematically underestimate cortical deformations during gyrification, registration approaches leveraging the full MRI sequence estimate spatiotemporal deformations more aligned with the fetal brain developmental trajectory.

Keywords: Registration · Cortical folding · Longitudinal fetal MRI.

1 Introduction

The human brain exhibits significant anatomical changes throughout life, with particularly pronounced global expansion during fetal development. Alongside volume growth, late gestation is characterised by the sudden, rapid folding of the cortical surface, known as gyrification [1]. Highly correlated with developmental age, cortical folding begins in the central regions and progressively extends toward the cortical lobes [8, 9], serving as a strong biomarker for the detection of atypical development [18].

High-resolution spatial information provided by Magnetic Resonance Imaging (MRI) combined with temporal analysis, offers clinicians valuable information for estimating morphological changes and thus the trajectory of typical brain development. Deformation estimation between images is typically achieved through registration approaches that compute either single or time-continuous transformations that maximise the correspondence between a deformed source image

and a reference image [3, 15, 6] or between the source image and a longitudinal MR sequence [12, 5, 10]. Pairwise methods iteratively optimise a similarity-based objective to obtain the optimal deformation for one image pair at a time. Recent deep-learning approaches [6, 12, 5] extend this paradigm by training neural networks on large datasets, reducing inference time while maintaining accuracy and enabling foundation models elaboration [15]. To ensure anatomical plausibility, optimal deformation aim to satisfy diffeomorphic properties through regularisation constraints [3, 15, 12] or a direct formalism [6, 5]. Such methods model deformation as a continuous-time trajectory between source and target images, driven by a velocity field that governs the transformation dynamics [2]. Stationary velocity fields (SVFs) have been used to reduce computational complexity [6, 11]. However, the capacity of these diffeomorphic approaches to accurately characterise neurodevelopmental dynamics during cortical gyrification has not yet been investigated.

This article addresses two questions related to modelling brain development: (1) How effective are diffeomorphic registration algorithms in capturing the complex anatomical deformations caused by gyrification? (2) How can multiple MRI scans, acquired over time, be temporally integrated to estimate these deformations accurately? We address these questions by comparing standard diffeomorphic pairwise and longitudinal registration and by investigating an alternative longitudinal SVF-based method.

Section 2 presents a diffeomorphic longitudinal approach derived from a pairwise registration SVF-based framework that integrates the entire MRI sequence to capture the non-linear brain deformations. Section 3 describes the experiments, including the datasets, the compared methods, the evaluation protocol, and presents / discusses the results. Section 4 provides concluding remarks.

2 Method

This Section presents a longitudinal registration method derived from a pairwise registration SVF-based framework. Section 2.1 introduces the pairwise registration SVF-based framework while Section 2.2 describes its longitudinal extension. Section 2.3 presents a method to account for non-linear brain development.

2.1 Pairwise SVF-based registration

Deep-learning diffeomorphic pairwise methods based on stationary velocity fields (SVFs) estimate a velocity field whose flow defines a time-continuous deformation aligning a source image onto a reference image using a weakly supervised approach. The deformation is modelled as the solution of an ordinary differential equation (ODE) restricted to a one-parameter subgroup of diffeomorphisms based on the SVF estimated by a network h_θ [11]. The SVF, denoted by $\mathbf{v}$, governs the flow equation yielding a time-continuous trajectory $\phi(\mathbf{x}, t)$ (also noted $\phi_t(\mathbf{x})$) with $t \in [0, 1]$ that represents all intermediate deformations from source to target, where $\phi(\mathbf{x}, 0) = \mathbf{x}$ for any $\mathbf{x}$ and $\phi(\mathbf{x}, 1)$ is the final deformation that

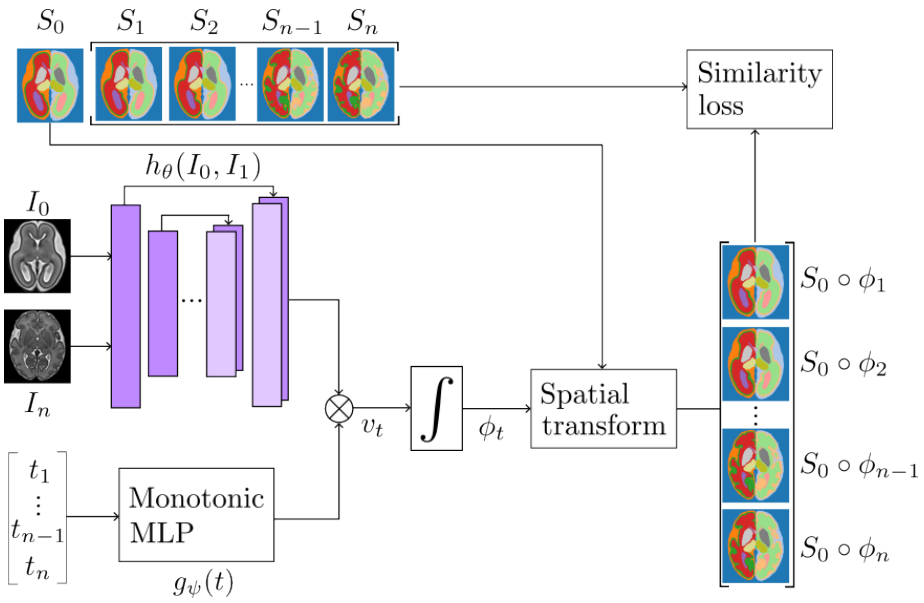

Fig. 1. Overview of our longitudinal method.

warps the source image to the target. The transformation is expressed via the Lie-group exponential:

$$\phi(\mathbf{x}, t) = \exp(v(\mathbf{x}) \times t). \tag{1}$$

This formulation allows an efficient computation of the continuous deformation as the exponential of the time-scaled SVF can be rapidly computed using a scaling-and-squaring algorithm. In the context of brain growth modelling, it provides an efficient description of the temporal evolution of brain deformation by interpolating between the source and the target.

2.2 Longitudinal SVF-based registration

The SVF-based deformation model allows the integration of additional time points to enforce spatio-temporal consistency with neurodevelopmental dynamics. We leverage the time-continuous diffeomorphic deformation modelling to integrate longitudinal MRI sequences $\mathcal{I} = \{I_0, I_1, \ldots, I_n\}$ or segmentation maps $\mathcal{S} = \{S_0, S_1, \ldots, S_n\}$ as temporal alignment checkpoints as illustrated in Figure 1. The estimated SVF is linearly modulated at the relative developmental ages (time steps) of the intermediate MRIs of the sequence to define the deformation that warps the initial image to the desired target images as formulated in Eq. (1). This yields a set of deformed images obtained by warping the initial image to the corresponding time points of the sequence. To maximise spatio-temporal consistency between the MRI sequence and the estimated deformations

at all checkpoints, we formulate a longitudinal optimisation problem to estimate the optimal network parameters $\theta^\star$ of the U-Net-like model [7], as follows:

$$\theta^\star = \arg_\theta \min \sum_{k=1}^{n} \mathcal{L}_{sim}(I_0 \circ \phi_{t_k}, I_k) + \lambda \mathcal{L}_{reg}(\phi_{t_k}) \tag{2}$$

where $\mathcal{L}_{sim}$ measures the similarity between each reference image I_k or segmentation S_k ($k \in [1, n]$) and the source I_0/S_0 warped by the deformation field ϕ_{t_k}. Here, t_k denotes the relative developmental age of I_k/S_k, normalised between the first and last time points. The similarity terms across all time steps are summed to encourage global spatio-temporal coherence and prevent overfitting to any single pairwise registration, while a regularisation term weighted by λ penalises non-diffeomorphic deformations. For regularisation, we adopt the cycle-consistency constraint introduced in SGDIR [12].

2.3 Non-linear temporal SVF-based modeling

To better accommodate the substantial temporal changes associated with non-linear fetal brain growth, we propose a non-linear modulation of SVF. This formulation relaxes the assumption of linear temporal evolution and enables more flexible modelling of developmental deformations over time. We introduce a network g_ψ thats learns a non-linear monotonic function of time, enabling it to modulate the temporal contribution of the SVF for the computation of deformations at each time interval. By construction, the network enforces temporal growth with respect to the boundary conditions $g_\psi(0) = 0$ and $g_\psi(1) = 1$, corresponding to the identity mapping and the final deformation along the geodesic path. The function g_ψ is implemented as a parametric multi-layer perceptron (MLP) with a softplus activation output layer to guarantee positivity. Growth is obtained by integrating the positive slope [14]. Finally, a normalisation by $g_\psi(t)/g_\psi(1)$ constrains the temporal factor to a fixed range between 0 and 1.

3 Experiments

3.1 Evaluation dataset

The experiments were conducted on two human fetal temporal atlases.
dHCP atlas [16] provides 16 longitudinal MRI templates spanning 21 to 36 gestational weeks, with isotropic resolution of 0.5 mm. Alongside the MRI templates, the dataset includes segmentation maps of 20 brain regions and deformation fields that model the morphological changes and local tissue transformations between consecutive time points. We employ these deformation fields as complementary information in our evaluation, and refer to them as "dHCP-def".
CRL atlas [4] contains 18 MRI templates with an isotropic spacing of 0.8 mm, covering up to 38 weeks. Segmentation masks of 19 brain structures are provided. However, the labelled regions are not consistent throughout the sequence,

as several structures visible in the earlier scans (weeks 21 to 37) are absent from the 38-week segmentation. This prevents the use of segmentation-based criteria during optimisation and of segmentation-based metrics during evaluation. We therefore excluded the last scan and limited our evaluation to weeks 21–37, so that all regions labelled at week 21 remain observable throughout the sequence and the anatomical correspondence between source and target images is preserved.

3.2 Compared methods

We compare the performances of widely used state-of-the-art registration approaches for capturing cortical gyrification, which we group into three families according to the temporal information they exploit.

- **Pairwise registration** methods seek the optimal deformation between each pair of images (I_0, I_k), independently of the rest of the sequence: SyN [3] from the ANTs toolbox, the foundation model uniGradICON [15], and an SVF-based baseline (SVF-PAIR) similar to VoxelMorph [6].
- **Interpolation-based** methods estimate a single deformation between the time points (I_0, I_n) and recover the intermediate ones by an interpolation process: SGDIR [12] and a temporal modulation of the SVF estimated by SVF-PAIR (SVF-INT).
- **Longitudinal** methods jointly exploit all images of the sequence to estimate a single temporally coherent trajectory: HH [10], NODER [5], and our SVF-based models, without the monotonic MLP (SVF-LIN, Section 2.2) and with it (SVF-MLP, Section 2.3).

3.3 Experimental protocol

To assess how effectively diffeomorphic registration algorithms capture the complex anatomical deformations induced by gyrification, we evaluate all methods in an instance-optimised setting, on each dataset separately. This protocol requires no train/test split, since our objective is to quantify how accurately the deformations of a given sequence are captured rather than to evaluate the generalisation ability of the methods. Our evaluation covers three complementary axes, namely alignment, folding and deformation regularity.

First, we evaluate anatomical alignment. The deformed images are compared visually with the target image. The registration accuracy of brain structures is then quantified from the segmentation maps, using the multi-class Dice score across all labelled regions of each atlas and the clDice score [13] on the cortex. Both evaluations compare the reference segmentations S_k ($k \in [1, n]$) and the source segmentation S_0 warped by the estimated deformation field ϕ_{t_k}. We analyse the average Dice and clDice score across the whole time series to examine the temporal trends, as well as at the last time point, which corresponds to the most challenging to estimate.

Second, we assess the degree of cortical folding using the 3D gyrification index (GI) [19], i.e. the ratio of the area of the mesh cortical surface to the area of

Table 1. Segmentation registration evaluation (Dice in white, clDice in grey). The subscript $1{:}n$ refers to averaged scores for all intermediate images, while the subscript n refers to the score for the last image. Best scores per method category in bold.

	dHCP atlas [16]				CRL atlas [4]			
	$Brain_{1:n}$	$Brain_n$	$Cortex_{1:n}$	$Cortex_n$	$Brain_{1:n}$	$Brain_n$	$Cortex_{1:n}$	$Cortex_n$
dHCP-def	92.14 ± 2.00	88.97	98.10 ± 1.90	94.53	–	–	–	–
SyN [3]	**97.81** ± 0.06	**96.56**	98.51 ± 1.91	94.06	**93.54** ± 1.05	**91.14**	93.87 ± 4.33	86.07
uniGradICON [15]	87.44 ± 4.83	78.01	84.83 ± 14.66	53.34	80.61 ± 5.04	71.47	79.83 ± 14.66	53.00
SVF-PAIR	95.55 ± 0.79	93.83	**99.23** ± 1.09	**95.80**	89.91 ± 0.77	88.20	**96.23** ± 1.61	**92.32**
SVF-INT	**86.23** ± 3.97	**93.83**	**77.78** ± 11.53	**95.80**	80.43 ± 4.35	88.20	75.73 ± 7.16	**92.32**
SGDIR [12]	85.49 ± 3.80	91.86	75.46 ± 11.51	91.15	**80.76** ± 4.23	**88.36**	**75.80** ± 6.88	91.30
HH [10]	85.43 ± 3.55	87.49	71.71 ± 9.96	72.93	78.15 ± 4.26	82.39	69.05 ± 7.58	74.03
NODER [5]	**93.82** ± 2.64	88.85	**95.58** ± 4.47	85.34	**89.43** ± 1.23	86.91	81.53 ± 3.43	75.78
SVF-LIN	89.70 ± 2.02	92.43	88.58 ± 5.41	92.07	83.96 ± 2.99	89.16	**82.93** ± 3.38	80.64
SVF-MLP	89.75 ± 2.17	**92.93**	88.41 ± 6.63	**92.91**	84.58 ± 2.78	**89.54**	82.76 ± 3.69	**80.72**

its smooth convex hull, at given gestation time [17]. The initial smooth brain is scaled to each folded brain to get the convex hull. All cortical surfaces, estimated and reference alike, were generated from the segmentation maps with 3D Slicer, ensuring an identical meshing procedure on both sides of the comparison.

Finally, we assess deformation regularity and the preservation of diffeomorphism by computing the maximal deformation magnitude and the number of voxels with a negative Jacobian determinant [5, 6, 15].

3.4 Training setup

We optimise the evaluated methods on the longitudinal MRI sequences using their original implementations, except for uniGradICON, which is applied in a zero-shot setting. This allows us to assess whether the rich representations learned by a large-scale pretrained model transfer to unseen fetal brain images, and whether they suffice to capture the large deformations involved. To ensure a fair comparison during the training step, we employ the same similarity loss across all compared methods, namely the mean squared error (MSE) between the warped and the reference one-hot encoded segmentation maps $S_{k,c}$ ($c \in [1, C]$), where C denotes the number of labels. No specific preprocessing was applied to the input images, except for intensity normalisation and zero-padding ensuring that all spatial dimensions are multiples of 32, as required by the network architectures.

Our SVF-based models, based on a original vanilla DynUnet [7] architecture without any modification, were trained using the Adam optimiser with a learning rate of 10^{-3} and a regularisation weight of $\lambda = 1\,000$. In the absence of a validation set, no early stopping criterion was applied and the number of epochs was fixed to 2 000, a value sufficiently large to reach a stable solution. These hyperparameters have been established empirically. Our source code is available at https://github.com/gis-beachild/longitudinal-svf.

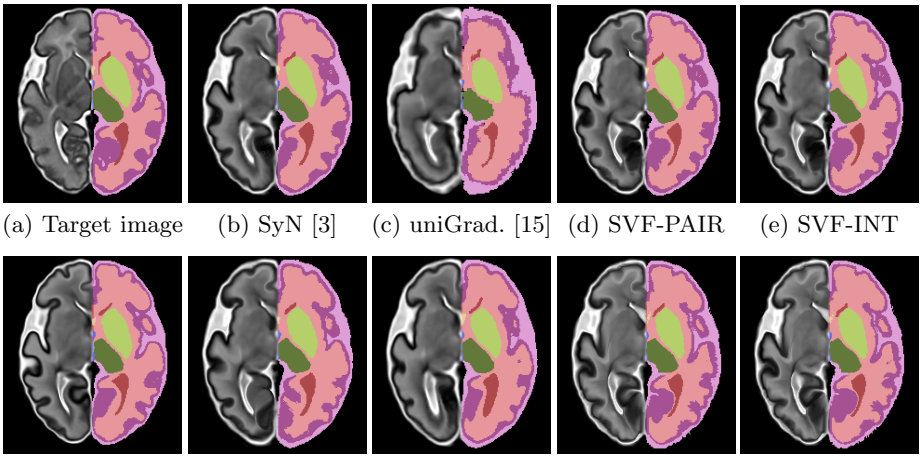

(a) Target image (b) SyN [3] (c) uniGrad. [15] (d) SVF-PAIR (e) SVF-INT

(f) SGDIR [12] (g) HH [10] (h) NODER [5] (i) SVF-LIN (j) SVF-MLP

Fig. 2. Visual comparison between the target (I_n/S_n) and the source (I_0/S_0) warped using the deformation fields estimated by each registration method. Images are shown on the left, segmentations on the right.

Table 2. Maximal displacement field magnitude and percentage of negative Jacobian determinants of the estimated displacement fields.

	dHCP atlas [16]		CRL atlas [4]	
	$\|\|\phi(\mathbf{x})\|\|$	$\det \mathcal{J} < 0$	$\|\|\phi(\mathbf{x})\|\|$	$\det \mathcal{J} < 0$
dHCP-def	4.67	0.00	–	–
SyN [3]	2.40	0.11	1.22	0.02
uniGradICON [15]	1.86	0.00	1.28	0.00
SVF-PAIR	1.87	0.01	1.18	0.00
SVF-INT	1.87	0.01	1.18	0.00
SGDIR [12]	2.26	0.17	0.94	0.02
HH [10]	3.39	0.10	2.23	0.00
NODER [5]	2.00	3.60	1.79	9.80
SVF-LIN	2.79	0.02	1.50	0.07
SVF-MLP	2.78	0.04	1.56	0.06

3.5 Results

A qualitative comparison between the estimated warped images and the ground-truth target is provided in Figure 2. We observe an absence of deformation for the foundation model uniGradICON, highlighting its inability to capture deformations outside its training domain. Table 1 presents the performance of the brain segmentation alignment. A first observation is that performance at the latest gestational age is consistently lower than the average over the full temporal sequence, highlighting the increased difficulty of modelling large deformations at later developmental stages. These differences are exacerbated for the cortex class. Pairwise registration methods consistently outperform longitudinal approaches,

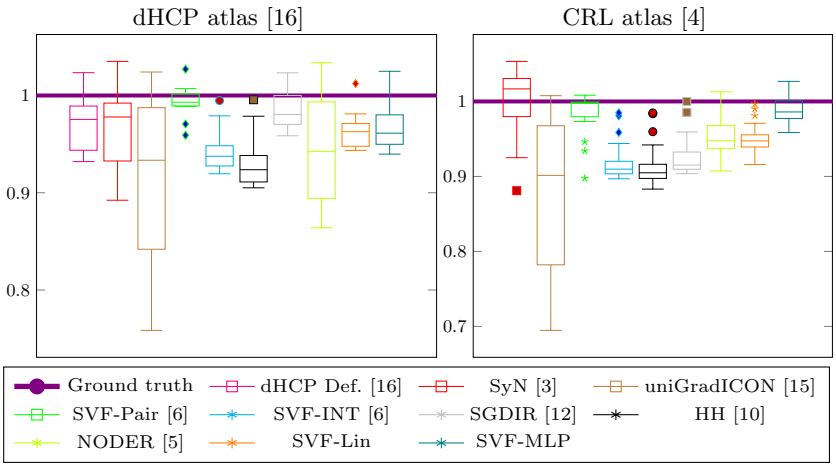

Fig. 3. Distribution of the normalized GI error between estimated and reference across the MRI sequence.

as they are optimised for a specific image rather than the entire MRI sequence. However, results for the last MRI show a smaller difference between registration paradigms in capturing deformation dynamics than on the average scores. Spatio-temporal methods based on pairwise interpolation, such as SVF-PAIR and SGDIR, produce notably lower cortical Dice scores and greater variability than longitudinal methods such as NODER and SVF-based longitudinal methods. Finally, the SVF-based longitudinal models reveal a limited performance improvement of the non-linear temporal modulation of the SVF.

Figure 3 presents box plots of the normalised error in the gyrification index. Scores are consistently below 1, indicating a global underestimation of folding compared to the target MRI. Among the compared methods, uniGradICON, SyN and NODER exhibit high variability across gestational ages. This behaviour shows an inability to maintain uniform registration performance throughout the sequence. Interpolation-based methods yield higher errors than other approaches, such as longitudinal methods. This observation highlights the importance of integrating the full MRI sequence to accurately model the highly non-linear deformation during the brain gyrification.

Table 2 summarises the characteristics of the estimated displacement fields, showing consistent magnitudes and percentages of negative Jacobians across both datasets. This table shows a higher magnitude for dHCP-def than for the compared methods, suggesting a registration-based underestimation of brain shape changes. This aspect is also present between longitudinal methods and pairwise approaches, with a lower amplitude for the latter. This may reflect a weakness in modelling the spatio-temporal growth of the brain. The Jacobian determinant analysis reveals few sign changes, except for NODER, highlighting

the ability of diffeomorphic methods to partially model cortical folding at the cost of producing undesirable transformation.

3.6 Discussion

In this study, we demonstrated that diffeomorphic registration algorithms exhibit contrasting capabilities in estimating the anatomical deformations, with a general underestimation of the cortical deformation during brain gyrification. This limitation may stem from the diffeomorphic property of image registration methods, where the regularisation term balances similarity and smoothness. Moreover, we observed that registration accuracy largely depends on the image registration paradigm. Pairwise methods outperform longitudinal methods. This gap narrows for temporally distant image pairs, where the deformations to estimate are larger. In contrast, accurately modelling the full spatio-temporal progression of cortical folding requires integration of the entire MRI sequence, as the emergence of sulci and gyri follows a highly non-linear temporal trajectory. Beyond paradigm-level patterns, several image registration methods led to notable observations. The foundation model exhibits a limitation in aligning a smooth brain to a folded brain without domain adaptation. The analysis of SVF-based longitudinal methods results reveals low variance in the gyrification index and the small variance in the Dice scores across all MRI time points in both evaluation datasets, but the introduction of non-linear temporal modulation does not lead to a significant improvement. Compared to the non-stationary velocity field approach (NODER), longitudinal SVF-based methods remain intrinsically limited in modelling the emergence of cortical folding patterns. Moreover, SVF-based approaches tend to estimate an average spatio-temporal developmental trajectory of the MRI sequence rather than capturing the underlying non-linear brain deformations.

4 Conclusion

In this article, we presented an analysis of the diffeomorphic image registration methods to model fetal human brain gyrification based on longitudinal MRI. Our analysis revealed that registration-based approaches underestimate cortical deformations, particularly at advanced gestational ages. We also investigated an integration approach of multiple MRI data via a longitudinal framework to capture the dynamics of neurological development. This approach, associated with a temporal non-linear modulation of the SVF, demonstrates slightly lower performance than the non-stationary velocity field method. Nevertheless, it has demonstrated remarkable properties, including less variability in registration accuracy over time, reflecting the modelling of the average spatiotemporal trajectory at all time points. This computationally efficient registration framework [2] may be particularly relevant for modelling spatio-temporal deformations in contexts with slower dynamics, such as brain plasticity or pathological changes.

Acknowledgments. The research leading to these results has received funding from ANR (HINT – ANR-22-CE45-0034; Chaire IA AI-4-CHILD – ANR-19-CHIA-0015). Additionally, this work was granted access to the HPC resources of IDRIS under the allocation 2023-AD010314332 made by GENCI.

Disclosure of Interests. The authors have no competing interests to declare that are relevant to the content of this article.

References

1. Armstrong, E., Schleicher, A., O., H., Curtis, M., Zilles, K.: The ontogeny of human gyrification. Cerebral Cortex **5**, 56–63 (1995)
2. Arsigny, V., Commowick, O., Pennec, X., Ayache, N.: A Log-Euclidean Framework for Statistics on Diffeomorphisms. In: Medical Image Computing and Computer-Assisted Intervention – MICCAI 2006, vol. 4190, pp. 924–931. Springer Berlin Heidelberg, Berlin, Heidelberg (2006)
3. Avants, B., Epstein, C., Grossman, M., Gee, J.: Symmetric diffeomorphic image registration with cross-correlation: Evaluating automated labeling of elderly and neurodegenerative brain. Medical Image Analysis **12**, 26–41 (2008)
4. Bagheri, M., Velasco-Annis, C., Wang, J., Faghihpirayesh, R., Khan, S., Calixto, C., Jaimes, C., Vasung, L., Ouaalam, A., Afacan, O., Warfield, S.K., Rollins, C.K., Gholipour, A.: An MRI atlas of the human fetal brain: Reference and segmentation tools for fetal brain MRI analysis. ArXiv p. 2508.15034 (2025)
5. Bai, H., Hong, Y.: NODER: Image sequence regression based on neural ordinary differential equations. In: MICCAI. vol. 15002, pp. 673–682 (2024)
6. Balakrishnan, G., Zhao, A., Sabuncu, M., Guttag, J., Dalca, A.V.: VoxelMorph: A learning framework for deformable medical image registration. IEEE Transactions on Medical Imaging **38**, 1788–1800 (2019)
7. Cardoso, M.J., Li, W., Brown, R., Ma, N., Kerfoot, E., Wang, Y., Murrey, B., Myronenko, A., Zhao, C., Yang, D., Nath, V., He, Y., Xu, Z., Hatamizadeh, A., Myronenko, A., Zhu, W., Liu, Y., Zheng, M., Tang, Y., Yang, I., Zephyr, M., Hashemian, B., Alle, S., Darestani, M.Z., Budd, C., Modat, M., Vercauteren, T., Wang, G., Li, Y., Hu, Y., Fu, Y., Gorman, B., Johnson, H., Genereaux, B., Erdal, B.S., Gupta, V., Diaz-Pinto, A., Dourson, A., Maier-Hein, L., Jaeger, P.F., Baumgartner, M., Kalpathy-Cramer, J., Flores, M., Kirby, J., Cooper, L.A.D., Roth, H.R., Xu, D., Bericat, D., Floca, R., Zhou, S.K., Shuaib, H., Farahani, K., Maier-Hein, K.H., Aylward, S., Dogra, P., Ourselin, S., Feng, A.: MONAI: An open-source framework for deep learning in healthcare. ArXiv p. 2211.02701 (2022)
8. Dubois, J., Benders, M., Borradori-Tolsa, C., Cachia, A., Lazeyras, F., Ha-Vinh Leuchter, R., Sizonenko, S.V., Warfield, S.K., Mangin, J.F., Hüppi, P.S.: Primary cortical folding in the human newborn: an early marker of later functional development. Brain **131**, 2028–2041 (2008)
9. Garel, C., Chantrel, E., Brisse, H., Elmaleh, M., Luton, D., Oury, J.F., Sebag, G., Hassan, M.: Fetal cerebral cortex: Normal gestational landmarks identified using prenatal MR imaging. American Journal of Neuroradiology **22**, 184–189 (2001)
10. Hadj-Hamou, M., Lorenzi, M., Ayache, N., Pennec, X.: Longitudinal analysis of image time series with diffeomorphic deformations: A computational framework based on stationary velocity fields. Frontiers in Neuroscience **10**, 236 (2016)

11. Lorenzi, M., Pennec, X.: Geodesics, parallel transport & one-parameter subgroups for diffeomorphic image registration. International Journal of Computer Vision **105**, 111–127 (2013)
12. Matinkia, M., Ray, N.: Learning diffeomorphism for image registration with time-continuous networks using semigroup regularization. ArXiv p. 2405.18684 (2025)
13. Shit, S., Paetzold, J.C., Sekuboyina, A., Ezhov, I., Unger, A., Zhylka, A., Pluim, J.P.W., Bauer, U., Menze, B.H.: clDice – A Novel Topology-Preserving Loss Function for Tubular Structure Segmentation. In: 2021 IEEE/CVF Conference on Computer Vision and Pattern Recognition (CVPR). pp. 16555–16564 (Jun 2021)
14. Sill, J.: Monotonic networks. In: Jordan, M., Kearns, M., Solla, S. (eds.) Advances in Neural Information Processing Systems. vol. 10. MIT Press (1997)
15. Tian, L., Greer, H., Kwitt, R., Vialard, F.X., San José Estépar, R., Bouix, S., Rushmore, R., Niethammer, M.: uniGradICON: A foundation model for medical image registration. MICCAI **15002**, 749–760 (2024)
16. Uus, A., Kyriakopoulou, V., Cordero Grande, L., Christiaens, D., Pietsch, M., Price, A., Wilson, S., Patkee, P., Karolis, S., Schuh, A., Gartner, A., Williams, L., Hughes, E., Arichi, T., O'Muircheartaigh, J., Hutter, J., Robinson, E., Tournier, J.D., Rueckert, D., Counsell, S., Rutherford, M., Deprez, M., Hajnal, J.V., Edwards, A.D.: Multi-channel spatio-temporal MRI atlas of the normal fetal brain development from the developing Human Connectome Project. G-Node (2023)
17. Wang, X., Lefèvre, J., Bohi, A., Al Harrach, M., Dinomais, M., Rousseau, F.: The influence of biophysical parameters in a biomechanical model of cortical folding patterns. Scientific Reports **11**, 7686 (2021)
18. Wu, J., Awate, S.P., Licht, D.J., Clouchoux, C., Du Plessis, A.J., Avants, B.B., Vossough, A., Gee, J.C., Limperopoulos, C.: Assessment of MRI-Based Automated Fetal Cerebral Cortical Folding Measures in Prediction of Gestational Age in the Third Trimester. American Journal of Neuroradiology **36**(7), 1369–1374 (2015)
19. Zilles, K., Armstrong, E., Schleicher, A., Kretschmann, H.J.: The human pattern of gyrification in the cerebral cortex. Anatomy and Embryology **179**, 173–179 (1988)